Monitoring tides, currents, and waves along coastal habitats using the Mini Buoy

Cai J. T. Ladd [1,2]*, **Alejandra G. Vovides** [2], **Marie-Christin Wimmler** [3], **Christian Schwarz** [4,5], **Thorsten Balke** [2,6]

[1]Department of Geography, Swansea University, Swansea, UK
[2]School of Geographical and Earth Sciences, University of Glasgow, Glasgow, UK
[3]Institute of Forest Growth and Forest Computer Sciences, Technische Universität Dresden, Tharandt, Germany
[4]Department of Civil Engineering, Hydraulics and Geotechnics, KU Leuven, Leuven, Belgium
[5]Department of Earth and Environmental Sciences, Geography and Tourism, KU Leuven, Leuven, Belgium
[6]Institute of Biology and Environmental Science, Carl von Ossietzky University of Oldenburg, Oldenburg, Germany

Abstract

Intertidal habitats are shaped by the actions of tides and waves which are difficult to monitor in shallow water. To address this challenge, the "Mini Buoy" and associated open-source App were recently developed for the low-cost and long-term monitoring of tidal inundation and current velocities simultaneously. The Mini Buoy is a bottom-mounted float that measures tilt to infer near-bed hydrodynamics. Here, we present significant updates to the Mini Buoy and App. Two new Mini Buoy designs were calibrated: the "Pendant" that requires minimal assembly for deployment, and the "B4+" that can also measure wave orbital velocity. Comparisons against industry-standard water-level and velocity sensors deployed in the field showed that each new design was effective at detecting tidal inundation (overall accuracy of 86–97%) and current velocities ($R^2 = 0.73$–0.91; accuracies of ± 0.14–0.22 m s^{-1}; detection limits between 0.02 and 0.8 m s^{-1}). The B4+ could reasonably measure wave orbital velocities ($R^2 = 0.56$; accuracies of ± 0.18 m s^{-1}; detection limits between 0.02 and 0.8 m s^{-1}). Reducing the sampling rate to prolong survey durations did not markedly reduce the precision of velocity measurements, except in the original Mini Buoy design (uncertainty increased by ± 2.11 m s^{-1} from 1 to 10 s sampling). The updated App enhances user experience, accepts data from any Mini Buoy design, is suitable for generic use across any tidal setting, and presents multiple options to understand and contrast local hydrodynamic regimes. Improvements to the Mini Buoy designs and App offer greater opportunities in monitoring hydrodynamics for purposes including ecosystem restoration and flood risk management.

*Correspondence: c.j.t.ladd@swansea.ac.uk

Coastal wetlands, including mangrove, saltmarsh, and seagrass habitats, are inherently dynamic systems shaped by the interaction of tidal inundation, currents, and waves with plants and their associated biogeomorphic features (Reed et al. 2018). The extent, density, and position of coastal wetlands within the tidal frame ultimately determines their biodiversity, ecosystem functions, and associated ecosystem services (Van Coppenolle and Temmerman 2020; Temmink et al. 2022). Hydrodynamic forcing drives coastal wetland dynamics across a range of spatial and temporal scales. Over spring-neap tidal cycles, the timing of inundation and magnitude of currents and waves determine whether pioneer mangrove seedlings establish or become dislodged (Balke et al. 2011). At estuarine scales, meandering tidal channels alter the exposure of saltmarshes to currents and waves that drive compensatory patterns of erosion and expansion (Ladd et al. 2021). Globally, increased tidal inundation by sea-level

rise poses an existential threat to coastal wetlands (Saintilan et al. 2020, 2022). Alongside remote sensing and numerical modeling tools (Cannon et al. 2020), long-term hydrodynamic monitoring is vital for assessing the resilience of intertidal wetlands in tackling the Climate and Biodiversity Crises (Waltham et al. 2020).

A suite of autonomous sensors are commercially available for monitoring fine-scale hydrodynamics along temporarily inundated coastlines with very shallow water. Acoustic Doppler Velocimeters (ADVs) and Acoustic Doppler Current Profilers (ADCPs) represent state-of-the-art technologies for measuring water movement (e.g., Nortek Vector and Eco profilers). Both use the doppler shift of sound waves reflected from suspended particles to measure 3D water flux (Woodward and Appell 1986). Non-vented pressure sensors, calibrated to detect waves and tides, use high-rate sampling in bursts to gather pressure data and automatically calculate wave properties (e.g., RBRsolo³). Other sensors use pressure transmitter (e.g., GE Druck PTX1830), impeller (e.g., Valeport Current Meters), or laser (e.g., RS Hydro Radar-Level sensors) technology to monitor tides, currents, and waves. All have been used to assess processes including wave attenuation by vegetation (Möller et al. 2014), morphological evolution of beaches (Rahbani et al. 2022), and spatial distribution of organisms (Pereda-Briones et al. 2018). Given that intertidal areas often have limited access with little nearby infrastructure, are exposed intermittently to both air and seawater, and often require deployments across multiple spring and neap cycles, instruments need to be stand-alone, waterproof, and durable. These requirements can amplify costs, time commitments, and need for additional expertise to rig appropriate monitoring stations with extended battery life for long-term monitoring. The short time that data can be gathered during high tides further skews the balance between risk of theft or damage and reward of retrieving usable data. Collectively, these limitations have hampered the large-scale and long-term surveying of hydrodynamic conditions along intertidal wetlands to date.

Micro-electromechanical system accelerometers have presented new opportunities for measuring the motion of water. Accelerometers consist of two miniature variable capacitance plates affixed with interlacing electrode "fingers." One plate can move while the other is fixed. Movement causes the fingers to move closer or pull apart, and the amount of displacement induces a differential capacitance between the fingers that is proportional to the acceleration applied (Polizzi et al. 2020). The accelerometer measures the pull of gravity along either of x–y–z axes depending on the orientation of the sensor, usually presented as G-force (where 1 G = 9.81 m s⁻²). When combined with microcontrollers, batteries, and data storage, acceleration loggers have been installed in moored floats to measure current velocity (e.g., MGL Marotte HS and Lowell Instruments TCM series and the open-source CavePearl; Beddows

and Mallon 2018) and turbulence (e.g., Underwater Relative Swell Kinetics Instrument; Figurski et al. 2011) using the drag-tilt principle (Marchant et al. 2014).

The Mini Buoy is an accelerometer-based drag-tilt sensor for the simultaneous monitoring of tidal inundation and current velocities in temporary shallow water (Balke et al. 2021). The Mini Buoy has been used to support research on the biomechanical properties of saltmarsh plants (Keimer et al. 2023), biodiversity distribution of mangroves (Hasibuan et al. 2021), and mangrove restoration potential in abandoned aquaculture ponds (Basyuni et al. 2022). The Mini Buoy overcomes many of the obstacles of conventional hydrodynamic equipment by being inexpensive to assemble, makes use of globally available material, and is small and thus suited for deployments along exposed coastlines. Despite these advantages, the Mini Buoy lacked the capacity to monitor wave exposure (a key parameter in coastal wetland dynamics), became brittle and prone to cracking over time due to UV exposure, would detach from the fishing swivel under high hydrological forcing, and lost mobility if sediment became trapped around the swivel mechanism.

To overcome these issues, we present here a reinforced Mini Buoy design that was calibrated to detect wave orbital velocity, as well as inundation status and current velocity for long-term deployments. We refer to the original and updated Mini Buoy designs as "B4" and "B4+," respectively, according to the name of the acceleration logger model used in each. We also present the calibration of another acceleration logger, the "Pendant," that is housed in a float as factory standard. The Pendant is therefore even simpler to assemble than the B4 and B4+ designs. Finally, we also demonstrate improved detection of partially inundated cases across all three designs, and update the original Mini Buoy App presented in Balke et al. (2021) that allows researchers and coastal managers alike to analyze and interpret data gathered by any Mini Buoy design. To the best of our knowledge, the B4+ is the first integrated low-cost logger for detecting inundation duration, current velocity, and wave orbital velocity simultaneously in shallow tidal environments. We believe improvements to the App will facilitate increased usage of Mini Buoys by managers, to assess suitability of a site for restoration of coastal wetlands. Finally, we highlight possible applications and key research questions in limnology and oceanography that the new Mini Buoy designs could address.

Materials and procedures

Materials

The B4 uses a waterproof MSR145W B4 acceleration data logger (MSR Electronics GmbH) wrapped in a plastic bag and secured inside a 50-mL self-standing centrifuge tube 115 mm in length (Corning CentriStarTM), made watertight by applying silicone sealant around the lid. Two holes are drilled into opposite ends of the self-standing skirt, to which fishing

swivels are attached. A third swivel connects the swivels to form a 55-mm-length tether which is clipped to a metal pole inserted into the ground. The total length and weight of the B4 design is 170 mm and 42.3 g, respectively (Fig. 1). The MSR145W B4 logger has an accuracy of ± 0.15 G, a maximum sampling rate of 50 Hz and preset sampling intervals between 1 and 10 s used in this study, and is fitted with a rechargeable lithium-ion battery.

The B4+ design also uses an MSR145W B4 acceleration data logger held inside a modified centrifuge tube. The tube is a UV-protected 50 mL design, 115 mm in length (Fisherbrand), with an M4 7-mm thread stainless steel eye bolt inserted through a hole drilled into the base of the tube and fixed in place with a nut. Shot weight (20 g) is added to the tube to reduce buoyancy (pretesting showed that adding weight increased the Buoy's sensitivity to waves and currents; see

Supporting Information Text S1). Floral foam is used to keep both the center of the shot mass at the bottom of the tube and the acceleration logger upright. To ensure watertightness, a rubber O-ring is inserted around the inner lid, silicone sealant is applied on the tube thread to seal the lid, and epoxy glue covers the eye bolt perforating the centrifuge tube at the bottom. The B4+ is anchored to the ground via a 40-mm chain link comprised of two 15 mm crimpled fishing line rings (American Fishing Wire Surflon nylon-coated 1×7 stainless leader fishing line, 250 lb test, and 1.9 mm diameter, with 4.2 mm diameter single-barrel nickel–copper alloy crimp sleeves fastened at each end to make the loop) tethered via cable tie to a metal pole inserted into the ground. Fishing line rings were preferable to fishing swivels (used in B4 and Pendant designs) since swivels occasionally became jammed with fine sediment (preventing free movement of the buoy) and
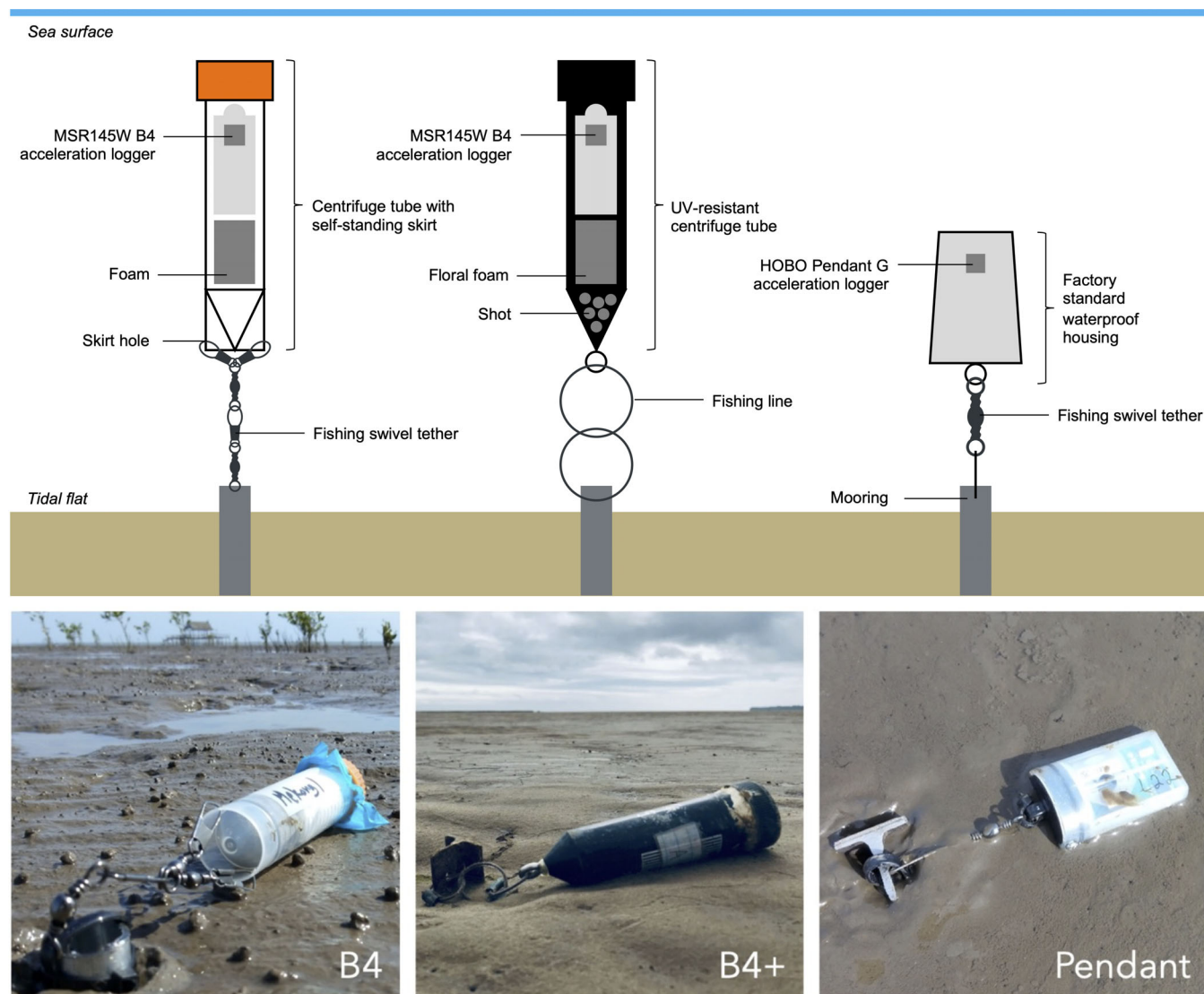

Fig. 1. Representation of fully submerged loggers and images of each logger deployed in situ for the B4, B4+, and Pendant Mini Buoy designs.

were more prone to detaching under high hydrological forcing. Fishing line rings were therefore better suited for deploying B4+ buoys for long periods of time in more dynamic environments. The total length and weight of the B4+ design is 155 mm and 60 g, respectively (Fig. 1).

The Pendant design is an integrated acceleration data logger 58 mm in length (Onset HOBO 2023) contained in a buoyant waterproof casing with mooring point as factory standard. The HOBO Pendant G is accurate to ± 0.075 G, has a sampling interval of 0.01 s to 18 h although is limited to 64 kb data storage, and is powered by a replaceable coin cell battery. A single barrel fishing swivel and fishing line is attached to the anchor point on the Pendant, and attached to a metal pole inserted into the ground via a cable tie to make a 50-mm-length tether. The total length and weight of the Pendant design is 108 mm and 19.9 g, respectively (Fig. 1).

Regardless of which Mini Buoy design is used, the operating principle is the same. An acceleration logger contained in a buoyant tube is anchored to the ground via a tether that allows free motion in all directions when inundated. In theory, any design that meets this specification can be used to create a Mini Buoy, provided the device is properly calibrated to measure hydrodynamics. Full specifications of each acceleration logger are shown in Supporting Information Table S1.

Procedures

Both the MSR145W B4 and HOBO Pendant G acceleration data loggers require dedicated connectors and software for configuration. The MSR145W B4 logger is supplied with USB cables and free MSR software. The current MSR software is only compatible with Windows operating systems In-Situ. The HOBO Pendant G logger requires a HOBO Waterproof Shuttle and coupler to connect to a PC. HOBOware software can be downloaded for free and is compatible with both macOS and Windows operating systems. MSR145W B4 is configured to only log acceleration along the *y*-axis between ranges of ± 2 G. HOBO Pendant G logger is configured to log acceleration along the *x*-axis only between ranges of ± 3 G. A metal pole between 300 and 700 mm in length is used to anchor Mini Buoys above the tidal flat.

We recommend that surveys last a minimum of 15 d to capture Spring-Neap tidal cycles along tidally influenced coastlines. The highest sampling frequency to achieve this minimum sampling duration (limited by memory) is 1.6 and 0.05 Hz (20 s) for MSR145W B4 and HOBO Pendant G loggers, respectively. To provide users with a range of survey durations, the MSR145W B4 has been calibrated for sampling rates between 1- and 10-s intervals every second, and 2-, 4-, 6-, 8-, and 10-min intervals for the HOBO Pendant G logger. The longest continuous deployment periods for the MSR145W B4 and HOBO Pendant G loggers are therefore 240 d (10 s sampling) and 1.2 yr (10 min sampling), respectively. Long-term deployments are also subject to battery life, which may vary depending on ambient temperatures. Examples of expected survey durations for given sampling rates are shown in Supporting Information Table S1.

Calibration

Each Mini Buoy was calibrated to detect inundation status and mean current velocity over 1-min intervals from single-axis acceleration time series. The B4+ design was also calibrated to measure mean wave orbital velocity over 10-min windows. Inundation status was classified as being either "non-inundated" (water levels are below a logger), "partially inundated" (water levels are between the base and length of a logger), or "fully inundated" (water levels exceed the length of a logger). The limited memory of the HOBO Pendant G negated its usefulness in measuring wave orbital velocities.

A representation of how hydrodynamics can be inferred from the Mini Buoys is shown in Fig. 2. All analyses were carried out in R (R Core Team 2022), and MATLAB 2022b (The MathWorks Inc. 2022) and the associated code are available in Supporting Information Texts S2 and S3, respectively.

Inundation status

Gravity-compensated acceleration values measured along a single axis and variance in those values over time provide two parameters for use in classifying whether a Mini Buoy is inundated or not. For acceleration values measured along a long-axis orientation, moving average and variance of acceleration ≈ 0 G would indicate a stationary Mini Buoy lying horizontally on an emersed tidal flat. Acceleration mean < 0 G and variance > 0 G would indicate a partially or fully submerged Mini Buoy that is "wobbling" due to the rise and fall of tides, or currents and wave action (Fig. 2). Pretesting has shown that moving mean and interquartile range (difference between the 75th and 25th percentiles) yield good separation of the data into point clouds for inundation status classification (*see* Supporting Information Text S2).

To relate water level to acceleration, training data were gathered for each Mini Buoy design at Percut Sei Tuan, Indonesia (3°43′22″N, 98°46′15″E), Caerlaverock, Scotland (54°58′05″N, 3°31′58″W), Black Scar, Wales (51°45′54″N, 4°26′12″W), and Skinflats, Scotland (56°03′22″N, 3°43′60″W). Further information about the surveys is provided in Supporting Information Table S2. For the B4, pressure data were gathered using an upward-facing Nortek Aquadopp 300-m current meter. Both the B4+ and Pendant loggers were calibrated against pressure data gathered from an In-Situ Rugged TROLL 100 pressure sensor mounted upright above the ground.

B4 and B4+ buoys sampled *y*-axis acceleration at 1 Hz, while Pendant buoys sampled at 0.1 Hz on the *x*-axis. Mean and interquartile range acceleration values were calculated over 1- and 10-min periods for the MSR145W B4 and HOBO Pendant G acceleration loggers, respectively. Pressure sensors logged every minute, corrected for atmospheric pressure, and converted to water level according to manufacturer's
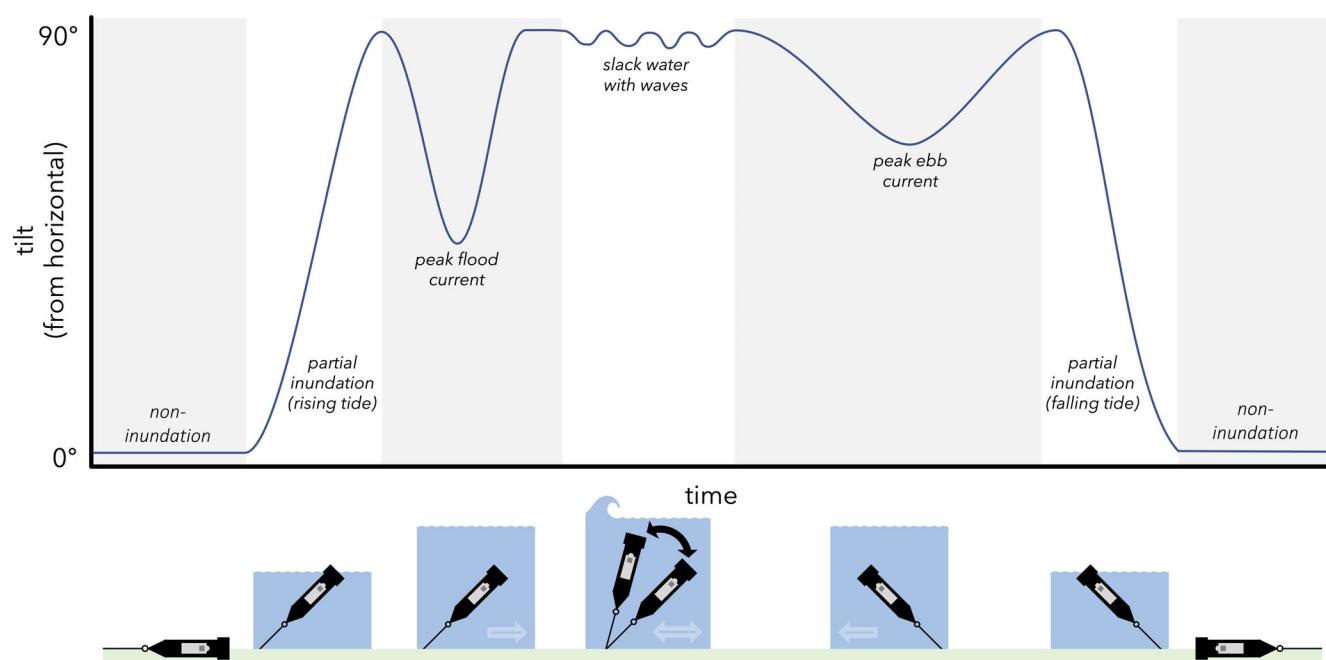
Fig. 2. A scenario representing tilt data gathered by a B4+ Mini Buoy during an inundation event that fully submerges the logger at a flood-dominant intertidal area.

instructions (Harris 2023). The water level was corrected for the height of the pressure sensors above the bed and set to start at the base of the Mini Buoy using a Leica RTK-GPS (B4+ and Pendant) or Leica Optical Level (B4) accurate to below 2 cm. A linear interpolation was used to predict water levels to match the sampling frequencies of the Mini Buoys. All negative water-level values were converted to 0. An inundation status was then assigned for when the Mini Buoy was emersed, partially inundated, or fully submerged. Acceleration values above 0 G were removed, to dismiss cases when a logger comes to rest below horizontal (e.g., in a depression caused by scouring around the mooring). Acceleration values below −1 G, indicating shocks in addition to acceleration due to logger tilt, were truncated. To do this, the accuracy of acceleration measures of each logger was taken into consideration (see Supporting Information Table S1) so that values were truncated to −1.15 and −1.075 G for the MSR145W B4 and HOBO Pendant G acceleration loggers, respectively. To aid interpretation, acceleration was converted to tilt from a horizontal position, where 0° represents a Mini Buoy lying horizontally on the tidal flat and 90° represents a buoy floating vertically in the water column. Tilt was calculated as:

$$\theta = \left(\frac{-180 \sin^{-1} a}{\pi} \right)$$

where θ is tilt (degrees) and a is gravity-compensated acceleration (G) measured along the long-axis of an accelerometer.

To identify the inundation status of a Mini Buoy without the need for local water-level data, a two-stage classification procedure was used. First, we trained machine learning techniques (Linear Discriminant Analysis for the B4 design and Quadratic Discriminant Analysis for B4+ and Pendant designs) to distinguish between "non-inundated" and "inundated" cases from moving mean tilt and interquartile range acceleration values over 1-min (B4 and B4+) and 2-min (Pendant) windows using the a priori classified data. We then divided "inundated" cases into "partially inundated" and "fully inundated" using the rapid transition in tilt of a Mini Buoy that occurs at the start and end of inundation events. An abrupt shift detection algorithm (Boulton and Lenton 2019) was used to detect the rapid transitions. The method fits a series of linear regression models along a time series, and records the gradient of each. Gradients that lie beyond ±3 median absolute deviations of the sample mean are given scores of 1 (positive gradient) or −1 (negative gradient) and divided by the number of linear models used to generate a detection score. Detectable shifts were assigned as partially inundated cases. A classifier built for each Mini Buoy design and the abrupt shift detection algorithm could then be used to predict the inundation status from acceleration data alone. Classifier and abrupt shift detection algorithms were applied using the "caret" and "asdetect" packages, respectively (Boulton and Lenton 2019; Kuhn et al. 2020).

Several "cleaning" steps were also implemented to correct any inundation status misclassifications. During inundation

events, points misidentified as non-inundated were converted to fully inundated if the duration of consecutive misclassified points were below a threshold period (20 min by default). Inundation events that lasted less than the threshold period were reclassified as partially inundated. Mini Buoys that reached a fully upright position at 90° were automatically classified as fully inundated. Inundation events were classified as partially inundated if the minimum tilt per event failed to cross a threshold value. Each processing step for classifying inundation status is shown in Fig. 3.

Current velocity

Calibration curves between tilt and current velocity were generated from data gathered by Mini Buoy and current meter arrays. The surveys were done in Percut Sei Tuan, Indonesia (3°43′22″N, 98°46′15″E), Black Scar, Wales (51°45′54″N, 4°26′12″W), and Skinflats, Scotland (56°03′22″N, 3°43′60″W). Further detail about each survey is available in Supporting Information Table S2. The B4 and B4+ buoys recorded acceleration at 1 Hz, while the Pendant sampled once every minute. The B4 buoy was calibrated using an upward-facing Nortek Aquadopp 300 m. "Diagnostic Mode" was used to

measure in 1025 sample bursts every hour at 1 Hz (internal sampling rate was 23 Hz). The measurement head was located 20 cm above the sediment surface, and blanking distance set to 35 cm. The B4+ buoy was calibrated using an upward-facing Acoustic Doppler Velocimeter (Nortek Vector), hereafter referred to as ADV. Height of the ADV pressure sensor and velocity cell being measured above the bed was 4 and 30 cm, respectively. Velocities were recorded at a rate of 16 Hz in 13-min bursts every 30 min. Nominal velocity range was set to 0.3 m s^{-1} and "Surf Zone" default settings were used. The Pendant design was calibrated using an upward-facing Nortek ECO taking velocity readings every 2 min. The lower sampling bin was used for surveying velocities nearest the ground. All Mini Buoys were deployed within 5 m of the current meters.

Tilt data from partially inundated Mini Buoys, or buoys that are close to a partially inundated state, would result in spurious tilt-velocity correlations and were removed. For the B4 design, this was done by first identifying the high tide of each inundation event, then selecting the first and last 50 min of data either side (Balke et al. 2021). For the B4+, acceleration values were selected to correspond with ADV velocity readings
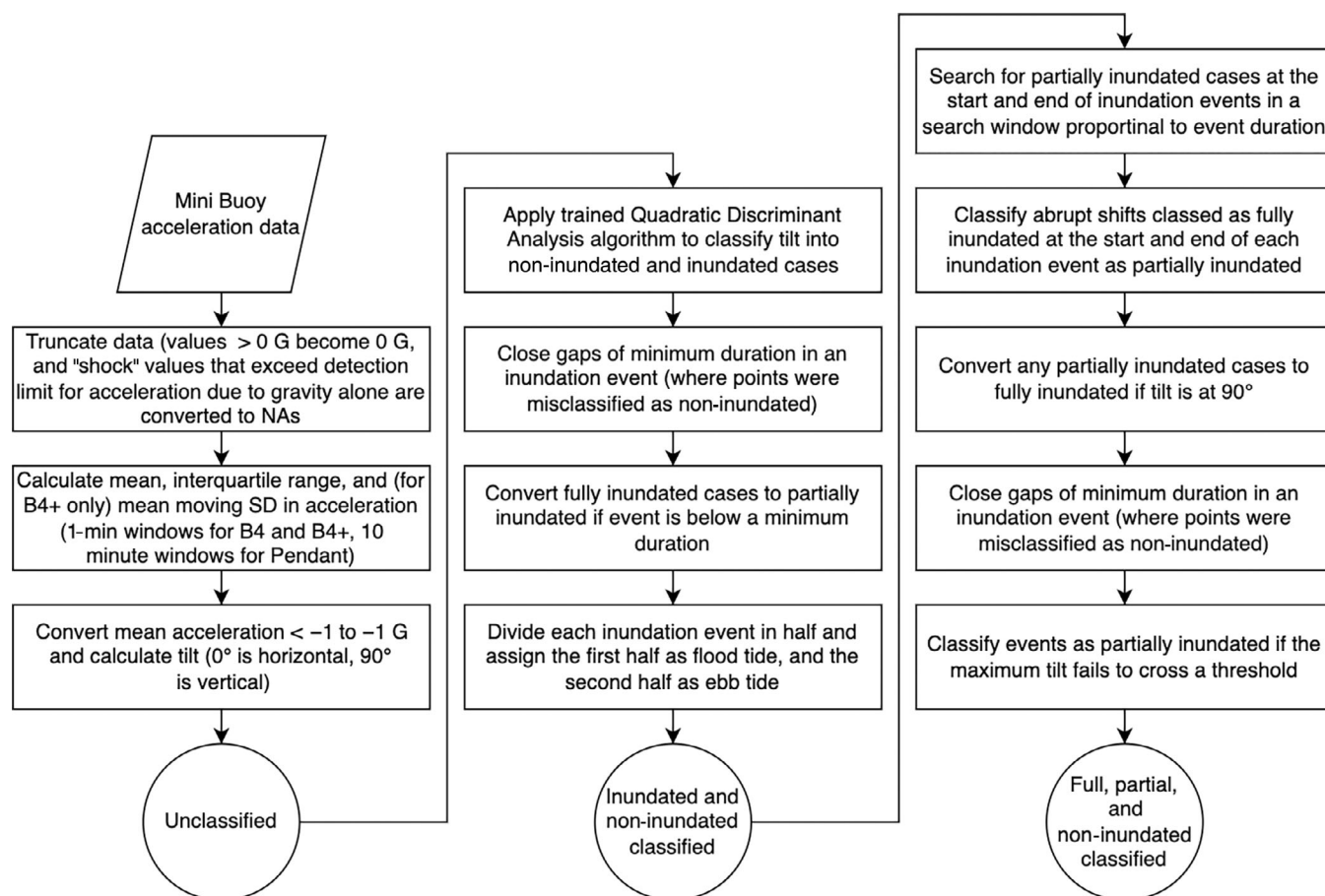

Fig. 3. Workflow to derive inundation status (non, partial, and full inundation) from acceleration data gathered by Mini Buoys.

that had an average normalized correlation score between receiver arms of greater than 75% (as recommended by the manufacturer). These values correspond to times when the ADV is fully inundated, and thus ensured only velocity and acceleration values were used for when the B4+ buoy was covered by at least 30 cm of water (i.e., the height of the water parcel above the bed measured by the ADV). Velocity magnitude of the vector sum (v_{xy} or v_{xyz}) across x (v_x), y (v_y), and for the ADV, z (v_z) axes were then calculated for each current meter at the sensing depth (between 30 and 55 cm above the tidal flat):

$$v_{xy} = \sqrt{\left(v_x^2 + v_y^2\right)}$$

$$v_{xyz} = \sqrt{\left(v_x^2 + v_y^2 + v_z^2\right)}$$

Calibration curves between tilt and current velocity were fitted with a 3rd-order polynomial regression for B4 and Pendant calibrations, and a linear regression for the B4+ design based on appropriate model fits (*see* Supporting Information Text S2). B4 and Pendant designs likely sample different proportions of the current velocity profile with changes in tilt, justifying the need for a polynomial fit (Balke et al. 2021). A linear regression was sufficient for the B4+ calibration, likely due to the increased sensitivity of the logger from the addition of ballast (*see* Supporting Information Text S1). The 95% prediction interval limits were calculated to quantify calibration uncertainty. A series of calibration curves were calculated to investigate how reducing acceleration sampling rate, and increasing the window over which mean tilt values were obtained, affected velocity calculation accuracy. For the B4 and B4+, sampling rates of 1–10 s and averaging window of 1, 5, 10, and 20 min were tested. For the Pendant, sampling rates of 2, 4, 6, 8, and 10 min and averaging window of 2, 5, 10, 20 min were tested.

Wave orbital velocity

A calibration curve between acceleration variance and wave orbital velocity was generated for the B4+ design. Data from two survey locations were used in the calibration: Caerlaverock, Scotland (54°58′05″N, 3°31′58″W), and Black Scar, Wales (51°45′54″N, 4°26′12″W). Further information about each survey site is given in Supporting Information Table S2. The first dataset was the same one used for the current velocity calibration (described in "Current velocity" section). The second dataset gathered at Caerlaverock marsh followed the same experimental design, although the ADV sampled at 1 Hz in 20-min bursts every 1 h. For the ADV deployed at Caerlaverock, the pressure sensor and velocity cell were 9 and 32 cm above the tidal flat, respectively. Near-bed velocities and surface-wave spectra were gathered from the ADV velocity and pressure sensors to estimate wave orbital velocities. Directional wave spectra were first estimated, then wave number and period

calculated to estimate orbital velocities (Wiberg and Sherwood 2008). *See* Supporting Information Text S3 for a validation of this approach. Prior to analysis, velocity data were filtered to remove values with an average beam correlation value of < 75% indicating partial inundation. Bursts that had > 5% of missing data were also removed. Rotated velocity vectors, u_r, v_r, and w_r, aligned with the main flow direction, were calculated from the x, y, and z velocity values recorded by the ADV (Lorke et al. 2013). Peak wave orbital velocity near the wave boundary layer, U_δ, was calculated as:

$$U_\delta = \frac{\pi H}{T \sinh(kh)}$$

where H is the significant wave height (m), h is the water depth (m), and T is the wave period (s) (Duvall et al. 2019). The wave number (m^{-1}), k, was calculated as:

$$k = \frac{2\pi}{L}$$

where L is the wavelength (m), calculated as:

$$L = \left(\frac{gT^2}{2\pi}\right) \tanh(kh)$$

Nominal number of output frequencies were 780 and 1000 for Black Scar and Caerlaverock sites, respectively. Low-frequency cutoff was set to 0.067 Hz (Chen et al. 2016), maximum value of factor scaling pressure to waves was 200, and minimum spectral level for computing direction and spreading was 0.03 m^2 Hz^{-1}. The calibration curve between the means of both 1-min moving standard deviation in acceleration (to detrend the impact of current velocity) and wave orbital velocity every 10 min was fitted with a linear regression based on appropriate model fits (*see* Supporting Information Text S2). The 95% prediction interval limits were calculated as a measure of uncertainty. Several calibration curves were fitted to determine the effect of reducing the sampling rate on calibration coefficients and uncertainty by downsampling the 1 Hz measurements of the B4+ every second from 1 to 10 s. Wave directional spectra extraction and processing from the ADV data were done using MATLAB 2022b (The MathWorks Inc. 2022), and the code to calculate the wave orbital velocity values from Acoustic Doppler Velocimeter data scripts are available in Supporting Information Text S3.

Assessment

Inundation status

Inundation status was identified correctly at rates of 86–97% across all Mini Buoy designs (Table 1). When considering the balanced accuracy scores of each inundation class, non-inundated cases were assigned correctly at rates above 86%

across all Mini Buoy designs. Fully inundated cases also scored highly for accuracy, except for B4+ where accuracy dropped to 81%. B4+ had higher accuracy at detecting partially inundated cases (80%) than both the B4 and Pendant designs (58% and 77%, respectively).

Due to potential inaccuracies with water levels (distances between water-level loggers and Mini Buoys) and elevation surveying during the inundation calibrations, we corroborated the inundation status classifications with a visual inspection of the individual tilt time series (by identifying timesteps where the logger was unequivocally moved from resting position). To further examine the performance of the classifier in contrasting tidal settings, we gathered tilt data using the B4+ in two deployments: in the breach site of a restored saltmarsh

in Cwm Ivy, south Wales (51°37′31″N, 4°14′47″W), and a wide and shallow channel flanking mangrove restoration planting sites in the Thai Binh Nature Reserve, northern Vietnam (20°34′42″N, 106°37′01″E). Cwm Ivy was characterized by strong flood and ebb current velocities with a rapid rise and fall of the tide, while Thai Binh had persistent shallow inundation, with a much more gradual rise and fall of the tide and low current velocities.

The classifier was consistently effective in distinguishing between non, partial, and full inundation (Fig. 4). Both sites exhibited two negative peaks per tide, characteristic of peak flood and ebb currents. Transitions before and after the flood and ebb tides, respectively were correctly captured as partial inundation (Fig. 4B,D). The gradual change in water level (especially for Thai Binh) likely accounted for some misclassification of partially inundated points as non-inundated. Crucially, however, fully inundated points were successfully differentiated from partially inundated cases, which is necessary to derive reliable calculations of current and wave orbital velocity.

Current velocity

Calibrations between Mini Buoy tilt and current velocity over 1-min (B4 and B4+) and 2-min (Pendant) windows (Fig. 5) yielded adjusted R^2 scores of between 0.73 and

Table 1. Percentage of overall accuracy and balanced accuracy scores for each inundation class per Mini Buoy design. "N," "P," and "F" represent non, partial, and full inundation cases, respectively.

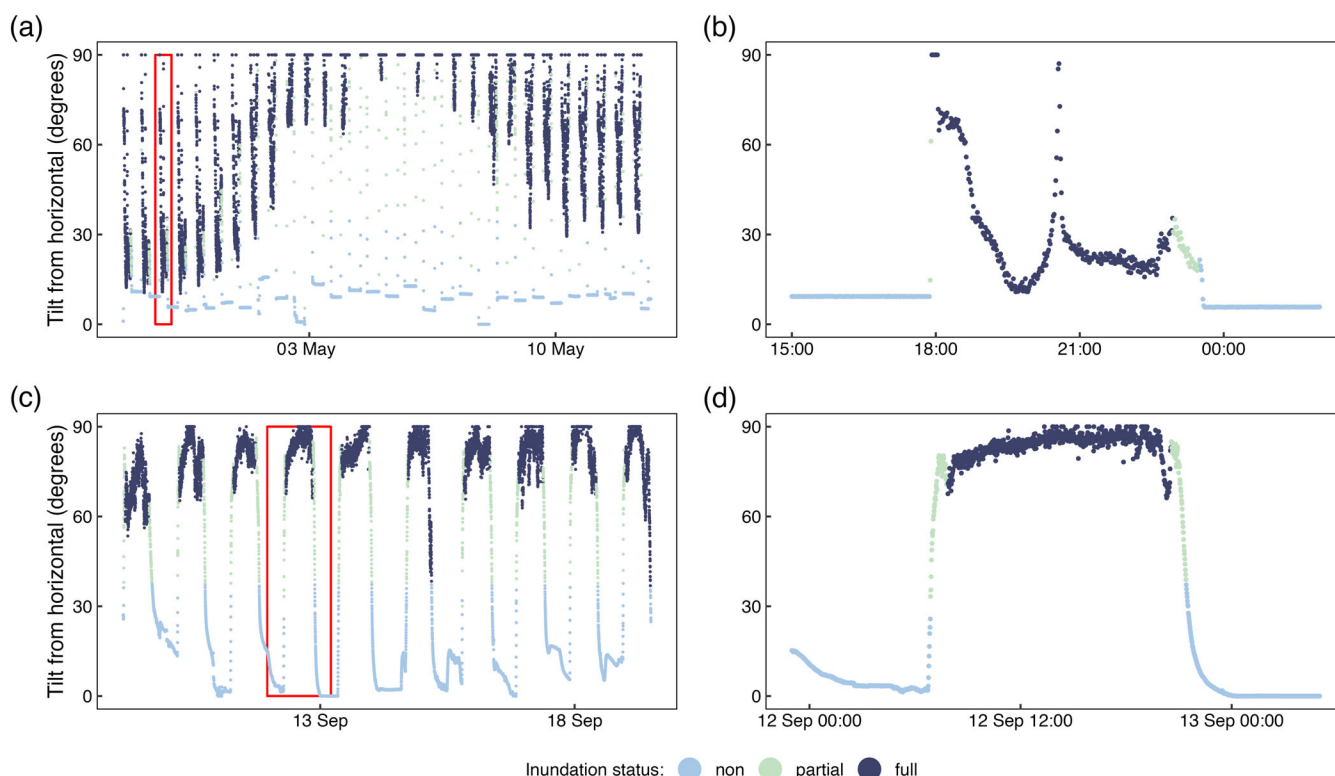| Design	Overall	N	P	F
B4	86	86	58	90
B4+	91	99	80	81
Pendant	97	98	77	94

Fig. 4. Tilt time series for a B4+ Mini Buoy from Cwm Ivy (**A**, the full duration of the survey between 27 April 2021 and 17 May 2021; **B**, a peak spring tide event) and Thai Binh (**C**, the full duration of the survey between 12 September 2022 and 13 September 2022; **D**, a single tide). Red bounding box indicates the values used for the single tide plots.
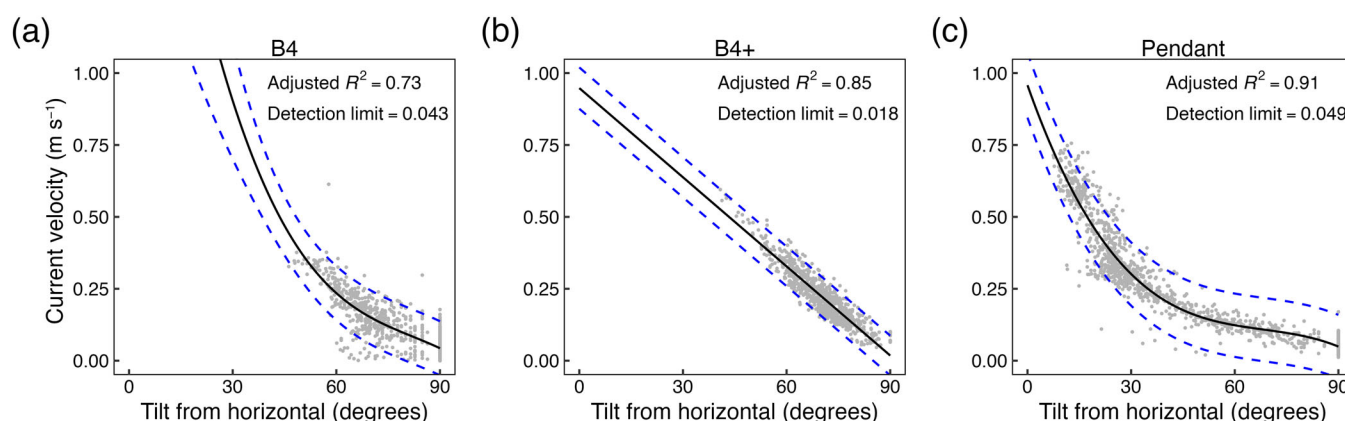
Fig. 5. Calibrations for converting mean tilt of (**A**) B4, (**B**) B4+, and (**C**) Pendant Mini Buoy designs to mean current velocity using 1 s sampling rate aggregated into 1-min intervals (B4 and B4+) or 1 min sampling rate aggregated into 2-min intervals (Pendant). Black solid lines represent the best-fit line through the data from polynomial (**A**, **C**) and linear (**B**) regression model. *p*-values are <0.001. Functions are (**A**) $y = 2.699 - 0.086x + 0.001x^2 - 4 \times 10^{-6}x^3$, (**B**) $y = 0.948 - 0.010x$, and (**C**) $y = 0.958 - 0.034x + 5 \times 10^{-4}x^2 - 2 \times 10^{-6}x^3$. Blue dashed lines represent upper and lower 95% prediction interval limits.

0.91. Detection limits were 0.043, 0.018, and 0.049 m s^{-1} for B4, B4+, and Pendant designs, respectively. While detection limits are lowest for B4+, sensitivity of the MSR145W B4 acceleration logger at near-vertical positions (tilt near 90° or acceleration values near −1 G) reduces; accounting for the gaps in data points near 90° for B4 and B4+ designs (Fig. 5A,B). The reduced range of values at 90° for the B4+ (and hence greater sensitivity in detecting low flow conditions) is likely due to the weight added (*see* Supporting Information Text S1). While adding weight to increase the B4+ sensitivity to detecting current velocities may have increased signal noise, averaging of acceleration values over time likely overcomes this issue and explains why the B4+ calibration is stronger than the B4 (Fig. 5). Mean 95% prediction interval widths over the range of tilt values recorded were 0.189, 0.138, and 0.220 m s^{-1} for B4, B4+, and Pendant designs, respectively. The range of current velocities sampled was constricted to ∼ 0.6 m s^{-1} for B4 and B4+, and ∼ 0.8 m s^{-1} for Pendant designs, respectively. While sheltered coastlines are unlikely to significantly exceed these values, we caution against extrapolating current velocities from Mini Buoy tilt beyond the range of the data. Each design could detect current velocity ranges that initiate scour around coastal vegetation (Bouma et al. 2009).

When considering the effect of sampling rate on the correlation strength between tilt and current velocity (Table 2), mean 95% prediction interval widths were over five times higher for B4 and rose by nearly 1.5 times for B4+ designs as the sampling rate decreased from 1 to 10 s. Adjusted R^2 scores and detection limits also weakened slightly. The increase in mean 95% prediction interval width at 10 s sampling for B4+ is still lower than B4 values at 1 s sampling. Reducing the sampling rate for the Pendant design had a negligible effect on correlation strength. Increasing the sampling window across

Table 2. Adjusted R^2, detection limit, and average uncertainty (mean 95% prediction interval width) scores for correlations between mean tilt and current velocity within 1-min (B4 and B4+) or 10-min (Pendant) windows across a range of acceleration sampling rates.

Design	Sampling rate (s)	Adjusted R^2	Detection limit (m s^{-1})	Mean 95% prediction interval width (m s^{-1})
B4	1	0.73	0.043	0.492
	2	0.73	0.043	0.640
	5	0.68	0.043	1.150
	10	0.71	0.047	2.600
B4+	1	0.85	0.018	0.138
	2	0.84	0.022	0.142
	5	0.80	0.035	0.166
	10	0.72	0.056	0.196
Pendant	120	0.92	0.048	0.203
	240	0.92	0.048	0.202
	360	0.93	0.046	0.201
	480	0.93	0.048	0.203
	600	0.91	0.050	0.224

which mean tilt and current velocities are taken (Table 3) resulted in a weaker correlation for B4 and B4+ designs, while having minimal effect on the Pendant design.

Wave orbital velocity

Calibrations between the mean values of both 1-min moving standard deviation in acceleration of the B4+ design and wave orbital velocity of the ADV over 10-min intervals produced an adjusted R^2 score of 0.56 (Fig. 6). The reasonable

Table 3. Adjusted R^2, detection limit, and average uncertainty (mean 95% prediction interval width) scores for correlations between tilt and current velocity at 1-s (B4 and B4+) or 2-min (Pendant) sampling rates averaged across a range of acceleration sampling windows.

Design	Sampling window (min)	Adjusted R^2	Detection limit (m s^{-1})	Mean 95% prediction interval width (m s^{-1})
B4	1	0.73	0.043	0.492
	5	0.68	0.039	0.994
	10	0.57	0.040	0.745
	20	0.45	0.046	0.447
B4+	1	0.85	0.018	0.138
	5	0.87	0.008	0.124
	10	0.85	−0.002	0.130
	20	0.71	0.028	0.170
Pendant	2	0.91	0.049	0.220
	5	0.92	0.047	0.213
	10	0.92	0.048	0.203
	20	0.92	0.047	0.204

Table 4. Adjusted R^2, detection limit, and average uncertainty (mean 95% prediction interval width) scores for correlations between the mean of 1-min moving standard deviation in acceleration and wave orbital velocity within 10-min windows for the B4+ across a range of acceleration sampling rates.

Sampling rate (a)	Adjusted R^2	Detection limit (m s^{-1})	Mean 95% prediction interval width (m s^{-1})
1	0.56	−0.007	0.172
2	0.57	−0.007	0.173
5	0.54	−0.004	0.178
10	0.50	0.001	0.187

wave orbital velocity should be made on this calibration. Whether this limit is sufficient to detect threshold velocities that trigger sediment mobilization at the bed depends on the biotic and abiotic nature of the tidal flat under scrutiny (Le Hir et al. 2007). Reducing the sampling rate from 1 to 10 s did reduce the strength of the correlation (Table 4).

The Mini Buoy App

An application allowing users to analyze Mini Buoy data was developed in R using the "shiny" package (Chang et al. 2021). This App is an update of the original programme presented in Balke et al. (2021) designed to support mangrove restoration. The new App provides users with greater functionality, faster processing, ability to analyze data from any of the three Mini Buoy designs, and a more user-friendly and generic interface suitable for any intertidal environment. The App allows users to examine results from two Mini Buoys at a time (identified as "reference" and "target" sites), as well as compare them statistically for a more definitive conclusion on whether sites differ hydrologically.

Users can navigate between the following pages:

- An "About" page describing how the Mini Buoys work and details about each Mini Buoy design, with a link to a handbook that provides more information on operating principles, assembly, configuration, deployment, and analysis (Fig. 7A).
- A "Settings" page to select where results should be exported, and options to change file formats, naming, and aesthetics.
- A "Data" page with "Upload" and "Filter" subpages. Users can upload either their own reference and target data, or example B4+ logger datasets. Once uploaded, tables appear, summarizing column names, sampling rate, survey length, monitoring period, mean and median acceleration, and amount of data recorded. Users can then select a start and end time for the survey, to remove irrelevant data (e.g., data logged prior to deployment and after retrieval, or non-overlapping dates between reference and target sites).
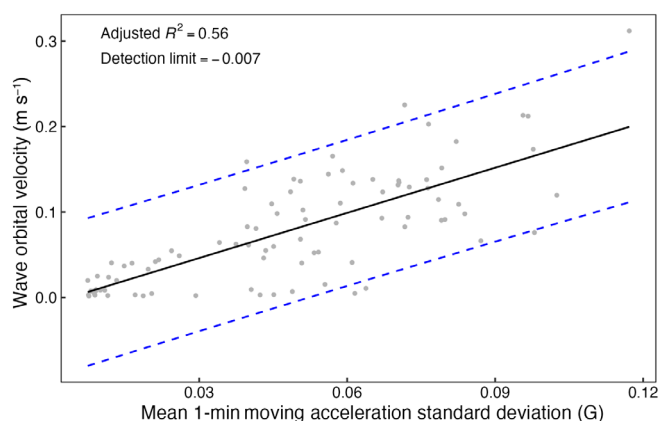
correlation between the sway of a Mini Buoy and wave orbital velocity indicates the B4+ is capable of measuring wave activity. The detection limit was slightly negative, at −0.007 m s^{-1}, likely because of the large uncertainty (0.178 m s^{-1} mean 95% prediction interval widths) over the range of standard deviation values. Wave orbital velocity accuracy is comparable to that of current velocity. The largest wave orbital velocity value observed was 0.31 m s^{-1}, setting a limit that extrapolations of

Fig. 6. Calibration for converting the mean of 1-min moving standard deviation in acceleration to wave orbital velocity as detected by the B4+ Mini Buoy design with a 1 s sampling rate. Black solid lines represent the best-fit line through the data from a linear regression model. *p*-value is <0.001. Function is $y = 1.761x - 0.007$. Blue dashed lines represent upper and lower 95% prediction interval limits.

(a)

(b)

(c)

(d)

Parameter	Units	Value
Survey days	[day]	24.57
Inundation events	[n]	31
Inundation duration	[h d^{-1}]	2.84
Emersion duration	[h d^{-1}]	21.16
Inundation proportion	[%]	11.85
Emersion proportion	[%]	88.15
Inundation frequency	[n d^{-1}]	1.26
Maximum Window of Opportunity	[day]	7.74
Upper 95th percentile ebb-flood ratio	[–]	1.09
Upper 95th percentile current velocity	[m s^{-1}]	0.27

(e)

Parameter	Units	Reference	Target	Meaningfully different	Target is
Inundation duration	[h d^{-1}]	2.59	2.84		8.8% higher
Inundation frequency	[n d^{-1}]	1.22	1.26		3.2% higher
Maximum Window of Opportunity	[day]	7.75	7.74		0.1% lower
Upper 95th percentile ebb-flood ratio	[–]	0.9	1.09	Yes	17.4% higher
Upper 95th percentile current velocity	[m s^{-1}]	0.39	0.27	Yes	44.4% lower
Mean current velocity	[m s^{-1}]	0.2	0.13	Yes	53.8% lower
Upper 95th percentile wave orbital velocity	[m s^{-1}]	0.2	0.18	No	11.1% lower
Mean wave orbital velocity	[m s^{-1}]	0.12	0.09	Yes	33.3% lower

Fig. 7. Selected pages of the Mini Buoy App. (**A**) "About," (**B**) "Data," and (**C**) "Hydrodynamics" pages, with zoomed-in results tables for a single Mini Buoy (**D**) and comparison between two Mini Buoys (**E**) taken from the "Hydrodynamics" page.

The unprocessed data can also be plotted as a line graph at custom time aggregations for further inspection (Fig. 7B). Both the (filtered) data and figure can be downloaded.

- A "Hydrodynamics" page with "Reference," "Target," and "Comparison" subpages. In the "Reference" and "Target" pages, a table presents several hydrodynamic parameters (Fig. 7D). Figures show time series of the raw data (colored by inundation status), daily inundation (Fig. 7C), current velocity, wave orbital velocity (B4+ only), ebb-flood currents profile for the longest inundation event, and Windows of Opportunity (the minimum inundation free period required for seedling establishment). For the "Comparison" page, tables (Fig. 7E), and figures compare hydrodynamic parameters between both reference and target sites, identifying by what proportion the target site is higher or lower than the reference, and whether that difference is statistically significant (the term "meaningfully different" is used, which may be a more

accessible term for non-specialists). Non-parametric Wilcoxon tests are used to test for statistical differences. Users can modify the default settings to improve the accuracy of results, and both data (Table S3) and figures can be downloaded.

The App follows the same operational steps outlined in Fig. 3 to calculate hydrodynamics. The App may be subject to updates in response to user feedback. See the data availability statement for how to access and use the App.

Discussion

Performance

Each Mini Buoy design is effective at detecting inundation (accuracy scores of 86–97%) and current velocities ($R^2 = 0.73$–0.91 for the highest sampling rates used here) in contrasting intertidal settings. Current velocities as low as 0.02 m s^{-1} and as high as 0.76 m s^{-1} could be detected. The B4+ is the first

integrated sensor that can also derive wave orbital velocities near the sediment surface ($R^2 = 0.56$) in addition to inundation and current velocities. The B4+ was able to detect wave orbital velocities between −0.01 and 0.31 m s^{-1}. There was no marked decline in the precision of inundation and current velocity measurements as sampling rate increases for the B4+ and Pendant designs. Increasing the time window over which tilt values are used in the calibration did not improve calibrations.

Mini Buoys have a number of advantages over conventional hydrodynamic sensing equipment. Capacity for continuous sampling up to 240 d for the B4 and B4+, and 1.2 yr for the Pendant desings enable the detailed monitoring of several spring-neap cycles, peak ebb-flood tides, and extreme storm, river flood, and infrequent emersion events. The low cost of globally available Mini Buoy materials allows low-budget projects to conduct hydrodynamic surveys, and offers the possibility for multipoint sampling when multiple loggers can be purchased. The low cost and small profile of the Mini Buoys also reduces the risk of losing equipment and thus a willingness to deploy them in more exposed settings (to physical forcing and heavy presence of people). For example, the rugged design of the B4+ was found to withstand flows exceeding 1 m s^{-1} at the Cwm Ivy site, and were successfully deployed for a year along Caerlaverock saltmarsh for a separate study. The addition of weight offers the possibility to use new acceleration data loggers that enter the market without the need to recalibrate the B4+ design, provided the logger fits inside the float, the weight is adjusted to the specifications outlined in Table S1 by adding or removing shot, and the center of mass of the buoy is preserved.

Applications

Within limnological and oceanographical research and application, there are several pressing issues that the new Mini Buoy designs are well suited to addressing. There remains an urgent need to characterize the hydrodynamic and hydrological suitability of intertidal environments for priority coastal habitat restoration through planting (Banerjee et al. 2023) or sowing (Bertelli et al. 2022), beyond generalist species-specific inundation thresholds (van Loon et al. 2016; Friess 2017; Kumbier et al. 2021) and to address the issue of hydrodynamic disturbance (Balke et al. 2014; Balke et al. 2016). The spatially replicated and simultaneous deployment of Mini Buoys across geomorphic settings would provide a database of average hydrodynamic conditions for practitioners to refer to when selecting optimal sites for restoration. The shift from expansion to erosion and vice versa is characterized by critical transitions (Wang and Temmerman 2013) that are notoriously difficult to detect in real-world settings (van Belzen et al. 2017). Mini Buoys could be used to detect and predict recovery thresholds (i.e., Windows of Opportunity) from bare to vegetated states with continuous in situ data on external forcing instead of relying on distant monitoring stations (Balke

et al. 2014). The open-source and low-cost nature of Mini Buoys are amenable for engagement of citizen science in research activities, improving literacy of coastal issues, and monitoring the success of conservation goals (Rahman et al. 2023). Mini Buoys would also be valuable in detecting the impact of episodic storm and river flood impacts (Leonardi et al. 2016), sediment fluxes when combined with turbidity sensors and field sampling (Ganju et al. 2013), and wave attenuation by vegetation (Möller et al. 2014); the monitoring of which have all hitherto been restricted in scale. Although we have so far limited our calibration for intertidal environments, Mini Buoys could be further calibrated for applications in rivers, lakes, and drainage channels.

Limitations and opportunities

Mini Buoys offer a novel tool for low-cost hydrodynamics monitoring. Yet, there remain limitations to their application. First, Mini Buoys need to be fully submerged before reliable current and wave orbital velocity values can be recorded. Mini Buoys require a minimum water depth of between 108 and 170 mm depending on design (*see* "Materials and procedures" section) to operate correctly. Processes such as wave scour in very shallow waters may therefore be missed.

Second, scouring and burial, entanglement with flotsam, and turbulence caused by nearby benthic organisms can impact on the reliability of current and wave orbital velocity measurements. To assist in detecting issues, the Mini Buoy App provides an interactive plot of the acceleration values to screen potential issues with the data.

The acceleration values plot is also important for addressing a third limitation of assessing whether partially inundated cases were successfully identified. The default parameters for detecting partial inundation may not be universally suitable and would require tuning by the user for optimal results. This limits the user-friendliness of the App, since additional effort may be required to understand the process by which partially inundated cases are identified (guidance available in the Mini Buoy Handbook), and to test which values yield the best results.

Fourth, no information is available on the direction of currents and wave orbitals. This limits the application of Mini Buoys in determining the direction of prevailing hydrological forcing, or in assessing sediment transport pathways. Mini Buoys also do not measure water level, only whether the logger was inundated or not. Mini Buoys are therefore unsuitable for measuring wave height, which is a function of water depth (Le Hir et al. 2007). While wave height may be more intuitively understood by coastal managers (especially in the context of the wave attenuation ecosystem service of coastal wetlands), wave orbital velocity at the bed provides a better understanding of seedling disturbance (Balke et al. 2011) or scour potential, and hence the potential for erosion or accretion at that location (Hu et al. 2015).

Loggers using micro-electromechanical systems are advancing rapidly, offering new opportunities to enhance the capacity of Mini Buoys in the future. For example, Inertial Measurement Units that comprise of three-axis accelerometer, magnetometer, and gyroscope sensors could be used in combination with optimal estimation algorithms (e.g., Kalman filter) to detect current and wave orbital direction as well as more precise velocities. New loggers entering the market are lower in cost, contain larger memory and battery capacity, use more sensitive micro-electromechanical systems, or provide additional features such as GPS and wireless data transfer that would enhance the capabilities of the Mini Buoy. Logger components, and instructions for their assembly, are also becoming more accessible. For example, Arduino microcontrollers and sensors can be assembled to create loggers that promote engagement and learning at substantially lower costs (Beddows and Mallon 2018). Future updates to the Mini Buoy App are also planned, such as enabling the batch processing of multiple Mini Buoy datasets, and hosting the App online to make it easier to use the App. Opportunities for improving the capabilities of the Mini Buoy and App would further aid the research and application goals of the limnology and oceanography community.

Data availability statement

Data used in the calibration of Mini Buoys for measuring inundation status, current velocity, and wave orbital velocity is available at https://doi.org/10.25405/data.ncl.25981414.v1 (related to Text S1), https://doi.org/10.25405/data.ncl.25981498.v1 (related to Text S2), and https://doi.org/10.25405/data.ncl.26097049.v1 (related to Text S3). A handbook on how to access the Mini Buoy App, as well as assemble, configure, deploy, and both export and analyze data from each Mini Buoy design is available at https://cailadd90.github.io/MiniBuoyHandbook/.

References

Balke, T., T. J. Bouma, E. M. Horstman, E. L. Webb, P. L. A. Erftemeijer, and P. M. J. Herman. 2011. Windows of opportunity: Thresholds to mangrove seedling establishment on tidal flats. Mar. Ecol. Prog. Ser. **440**: 1–9. doi:10.3354/meps09364

Balke, T., P. M. J. Herman, and T. J. Bouma. 2014. Critical transitions in disturbance-driven ecosystems: Identifying windows of opportunity for recovery. J. Ecol. **102**: 700–708. doi:10.1111/1365-2745.12241

Balke, T., M. Stock, K. Jensen, T. J. Bouma, and M. Kleyer. 2016. A global analysis of the seaward salt marsh extent: The importance of tidal range. Water Resour. Res. **52**: 3775–3786. doi:10.1002/2015wr018318

Balke, T., A. Vovides, C. Schwarz, G. L. Chmura, C. Ladd, and M. Basyuni. 2021. Monitoring tidal hydrology in coastal wetlands with the "Mini Buoy": Applications for mangrove restoration. Hydrol. Earth Syst. Sci. **25**: 1229–1244. doi:10.5194/hess-25-1229-2021

Banerjee, S., C. J. T. Ladd, A. Chanda, S. Shil, T. Ghosh, A. Large, and T. Balke. 2023. Securing the sustainable future of tropical deltas through mangrove restoration: Lessons from the Indian Sundarban. One Earth **6**: 190–194. doi:10.1016/j.oneear.2023.02.015

Basyuni, M., R. Amelia, D. Suryanto, I. E. Susetya, and Y. Bimantara. 2022. Empowerment of abandoned ponds for sustainable mangrove rehabilitation activities in Percut Sei Tuan, Deli Serdang, Indonesia. J. Sylva Indonesiana **5**: 137–147. doi:10.32734/jsi.v5i02.8727

Beddows, P. A., and E. K. Mallon. 2018. Cave Pearl Data Logger: A flexible Arduino-based logging platform for long-term monitoring in harsh environments. Sensors **18**: 530. doi:10.3390/s18020530

Bertelli, C. M., H. J. Stokes, J. C. Bull, and R. K. F. Unsworth. 2022. The use of habitat suitability modelling for seagrass: A review. Front. Mar. Sci. **9**: 997831. doi:10.3389/fmars.2022.997831

Boulton, C.A., Lenton, T.M. 2019. asdetect: A method for detecting abrupt shifts in time series. R package version 1. Available from https://github.com/caboulton/asdetect, DOI: 10.1186/s12913-019-4762-1

Bouma, T. J., M. Friedrichs, P. Klaassen, B. K. van Wesenbeeck, F. G. Brun, S. Temmerman, M. M. van Katwijk, G. Graf, and P. M. J. Herman. 2009. Effects of shoot stiffness, shoot size and current velocity on scouring sediment from around seedlings and propagules. Mar. Ecol. Prog. Ser. **388**: 293–297. doi:10.3354/meps08130

Cannon, D., K. Kibler, M. Donnelly, G. McClenachan, L. Walters, A. Roddenberry, and J. Phagan. 2020. Hydrodynamic habitat thresholds for mangrove vegetation on the shorelines of a microtidal estuarine lagoon. Ecol. Eng. **158**: 106070. doi:10.1016/j.ecoleng.2020.106070

Chang, W., and others. 2021. shiny: Web application framework for R. R package version 1.0.5. doi:10.32614/CRAN.package.shiny

Chen, Y., Y. Li, T. Cai, C. Thompson, and Y. Li. 2016. A comparison of biohydrodynamic interaction within mangrove and saltmarsh boundaries. Earth Surf. Process. Landf. **41**: 1967–1979. doi:10.1002/esp.3964

Duvall, M. S., P. L. Wiberg, and M. L. Kirwan. 2019. Controls on sediment suspension, flux, and marsh deposition near a bay-marsh boundary. Estuar. Coasts **42**: 403–424. doi:10.1007/s12237-018-0478-4

Figurski, J. D., D. Malone, J. R. Lacy, and M. Denny. 2011. An inexpensive instrument for measuring wave exposure and water velocity. Limnol. Oceanogr. Methods **9**: 204–214. doi:10.4319/lom.2011.9.204

Friess, D. A. 2017. J.G. Watson, inundation classes, and their influence on paradigms in mangrove forest ecology. Wetlands **37**: 603–613. doi:10.1007/s13157-016-0747-6

Ganju, N. K., N. J. Nidzieko, and M. L. Kirwan. 2013. Inferring tidal wetland stability from channel sediment fluxes: Observations and a conceptual model. Case Rep. Med. **118**: 2045–2058. doi:10.1002/jgrf.20143

Harris, R. D. 2023. Water level accuracy and correcting for errors due to gravitational acceleration and liquid density. Technical Note No. 001. In-Situ Inc. Available from https://in-situ.com/uk/support/documents/water-level-accuracy-and-correcting-for-errors-due-to-gravitational-acceleration-and-liquid-density-tech-note

Hasibuan, I. M., R. Amelia, Y. Bimantara, I. E. Susetya, A. Susilowati, and M. Basyuni. 2021. Vegetation and macrozoobenthos diversity in the Percut Sei Tuan mangrove forest, North Sumatra, Indonesia. Biodiversitas **22**: 5600–5608. doi:10.13057/biodiv/d221245

Hu, Z., Z. B. Wang, T. J. Zitman, M. J. F. Stive, and T. J. Bouma. 2015. Predicting long-term and short-term tidal flat morphodynamics using a dynamic equilibrium theory. Case Rep. Med. **120**: 1803–1823. doi:10.1002/2015JF003486

Keimer, K., V. Kosmalla, I. Prüter, O. Lojek, M. Prinz, D. Schürenkamp, H. Freund, and N. Goseberg. 2023. Proposing a novel classification of growth periods based on biomechanical properties and seasonal changes of *Spartina anglica*. Front. Mar. Sci. **10**: 1095200. doi:10.3389/fmars.2023.1095200

Kuhn, M., and others. 2020. caret: Classification and regression training. R package version 6.0-94. doi:10.32614/CRAN.package.caret

Kumbier, K., M. G. Hughes, K. Rogers, and C. D. Woodroffe. 2021. Inundation characteristics of mangrove and saltmarsh in micro-tidal estuaries. Estuar. Coast. Shelf Sci. **261**: 107553. doi:10.1016/j.ecss.2021.107553

Ladd, C. J. T., M. F. Duggan-Edwards, J. F. Pagès, and M. W. Skov. 2021. Saltmarsh resilience to periodic shifts in tidal channels. Front. Mar. Sci. **8**: 757715. doi:10.3389/fmars.2021.757715

Le Hir, P., Y. Monbet, and F. Orvain. 2007. Sediment erodability in sediment transport modelling: Can we account for biota effects? Cont. Shelf Res. **27**: 1116–1142. doi:10.1016/j.csr.2005.11.016

Leonardi, N., N. K. Ganju, and S. Fagherazzi. 2016. A linear relationship between wave power and erosion determines salt-marsh resilience to violent storms and hurricanes. Proc. Natl. Acad. Sci. USA **113**: 64–68. doi:10.1073/pnas.1510095112

Lorke, A., D. F. McGinnis, and A. Maeck. 2013. Eddy-correlation measurements of benthic fluxes under complex flow conditions: Effects of coordinate transformations and averaging time scales. Limnol. Oceanogr. Methods **11**: 425–437. doi:10.4319/lom.2013.11.425

Marchant, R., T. Stevens, S. Choukroun, G. Coombes, M. Santarossa, J. Whinney, and P. Ridd. 2014. A buoyant tethered sphere for marine current estimation. IEEE J. Ocean. Eng. **39**: 2–9. doi:10.1109/JOE.2012.2236151

Möller, I., and others. 2014. Wave attenuation over coastal salt marshes under storm surge conditions. Nat. Geosci. **7**: 727–731. doi:10.1038/ngeo2251

Onset HOBO. 2023. HOBO pendant G data logger (UA-004-64) white paper. Onset HOBO. Available from https://onsetcomp.com/resources/documentation/16920-pendant-g-white-paper

Pereda-Briones, L., E. Infantes, A. Orfila, F. Tomas, and J. Terrados. 2018. Dispersal of seagrass propagules: Interaction between hydrodynamics and substratum type. Mar. Ecol. Prog. Ser. **593**: 47–59. doi:10.3354/meps12518

Polizzi, J.-P., B. Fain, and F. Maspero. 2020. Accelerometer, p. 879–898. *In* M. T. M. Paulasto-Krockel, M. Petzold, H. Theuss, T. Motooka, and V. Lindroos [eds.], Handbook of silicon based MEMS materials and technologies, 3rd ed. Elsevier. doi:10.1016/B978-0-12-817786-0.00045-1

R Core Team. 2022. R: A language and environment for statistical computing. R Foundation for Statistical Computing, Available from https://www.r-project.org/

Rahbani, M., A. Vila-Concejo, T. E. Fellowes, S. L. Gallop, L. Winkler-Prins, and J. L. Largier. 2022. Spatial patterns in wave signatures on beaches in estuaries and bays. Geomorphology **398**: 108070. doi:10.1016/j.geomorph.2021.108070

Rahman, M. F., and others. 2023. Locally led adaptation is key to ending deforestation. One Earth **6**: 81–85. doi:10.1016/j.oneear.2023.01.011

Reed, D., B. van Wesenbeeck, P. M. J. Herman, and E. Meselhe. 2018. Tidal flat-wetland systems as flood defenses: Understanding biogeomorphic controls. Estuar. Coast. Shelf Sci. **213**: 269–282. doi:10.1016/j.ecss.2018.08.017

Saintilan, N., N. S. Khan, E. Ashe, J. J. Kelleway, K. Rogers, C. D. Woodroffe, and B. P. Horton. 2020. Thresholds of mangrove survival under rapid sea level rise. Science **368**: 1118–1121. doi:10.1126/science.aba2656

Saintilan, N., and others. 2022. Constraints on the adjustment of tidal marshes to accelerating sea level rise. Science **377**: 523–527. doi:10.1126/science.abo7872

Temmink, R. J., and others. 2022. Recovering wetland biogeomorphic feedbacks to restore the world's biotic carbon hotspots. Science **376**: eabn1479. doi:10.1126/science.abn1479

The MathWorks Inc. 2022. MATLAB version R2022b. Natick Massachusetts, Available from https://www.mathworks.com

van Belzen, J., and others. 2017. Vegetation recovery in tidal marshes reveals critical slowing down under increased inundation. Nat. Commun. **8**: 15811. doi:10.1038/ncomms15811

Van Coppenolle, R., and S. Temmerman. 2020. Identifying global hotspots where coastal wetland conservation can contribute to nature-based mitigation of coastal flood risks. Global Planet. Change **187**: 103125. doi:10.1016/j.gloplacha.2020.103125

van Loon, A. F. V., B. T. Brake, M. H. J. V. Huijgevoort, and R. Dijksma. 2016. Hydrological classification, a practical tool for mangrove restoration. PLoS One **11**: e0150302. doi:10.1371/journal.pone.0150302

Waltham, N. J., and others. 2020. UN Decade on Ecosystem Restoration 2021–2030—What chance for success in restoring coastal ecosystems? Front. Mar. Sci. **7**: 71. doi:10.3389/fmars.2020.00071

Wang, C., and S. Temmerman. 2013. Does biogeomorphic feedback lead to abrupt shifts between alternative landscape states?: An empirical study on intertidal flats and marshes. Case Rep. Med. **118**: 229–240. doi:10.1029/2012JF002474

Wiberg, P. L., and C. R. Sherwood. 2008. Calculating wave-generated bottom orbital velocities from surface-wave parameters. Comput. Geosci. **34**: 1243–1262. doi:10.1016/j.cageo.2008.02.010

Woodward, W., and G. Appell. 1986. Current velocity measurements using acoustic doppler backscatter: A review. IEEE J. Ocean. Eng. **11**: 3–6. doi:10.1109/JOE.1986.1145147

Acknowledgments

Conflict of Interest

None declared.